DALTON
FULL PAPER

The systematic influence of tripodal ligands on the catechol cleaving activity of iron(III) containing model compounds for catechol 1,2-dioxygenases †

Matthias Pascaly, Mark Duda, Florian Schweppe, Kristin Zurlinden, Felizitas K. Müller and Bernt Krebs*

Anorganisch-Chemisches Institut der Westfälischen Wilhelms-Universität Münster, Wilhelm-Klemm-Straße 8, D-48149 Münster, Germany. Fax: (+49) 251-833 8366; E-mail: krebs@uni-muenster.de

Received 23rd October 2000, Accepted 25th January 2001
First published as an Advance Article on the web 26th February 2001

A series of mononuclear iron(III) complexes as functional and structural model compounds for intradiol cleaving catechol dioxygenases were synthesized. For all model compounds the iron(III) cores are in a distorted octahedral environment derived from tripodal tetradentate N_4-donor ligands and a catechol. Model complexes for enzyme–substrate adducts were characterized by spectroscopic and electrochemical methods, and in four cases by single-crystal X-ray crystallography. The systematic variation of one ligand arm in the structurally characterized complexes yields a different steric shielding of the iron(III) center, significantly influencing the bonding of the catechol substrate and the subsequent reaction with dioxygen. The spectroscopic features and catechol cleaving activities of *in situ* generated complexes with the above ligands were probed. All complexes are highly reactive towards intradiol cleavage of various catechols in the presence of air. The catechol 1,2-dioxygenase reaction depends on the redox potential of both the iron(III) complex and the catechol derivative as well as the steric demand of the tripodal ligand. Some complexes show high catalytic activities with yields up to 84% with respect to aerial cleavage of catechols.

Introduction

Catechol dioxygenases are mononuclear non-heme iron enzymes that can be isolated from bacteria.[1] These enzymes have attracted considerable attention due to their key role in the metabolism of aromatic compounds. The catalytic cleavage of catechols yields aliphatic products by insertion of both atoms of dioxygen into the aromatic ring.[1–3] Traditionally, catechol dioxygenases are subdivided into intradiol and extradiol cleaving enzymes according to their catalysis of the ring cleavage between or outside the two *ortho*-hydroxo groups (Fig. 1).[4] The intradiol cleaving enzymes (catechol 1,2-dioxygenases) contain iron(III) in their active site whereas extradiol cleaving dioxygenases (catechol 2,3-dioxygenases) possess an iron(II) center.[5]

In the first step of the proposed mechanism (Fig. 2) of catechol 1,2-dioxygenases the substrate binds to the metal site. An equilibrium is suggested between an iron(III) catecholate complex and an iron(II) semiquinone tautomer due to the electron accepting character of the iron(III) core. An increased semiquinone character of the intermediate leads to a more favorable attack of dioxygen at the enzyme–substrate complex. In the next step oxygen binds end-on to the semiquinone and, upon ring closure, an iron(III)–peroxo species is formed. In a Criegee-type rearrangement the peroxo adduct yields derivatives of muconic acid anhydride.[1,6] This mechanism describes a substrate activation due to electron transfer from the catecholate to iron(III).[6,7] Very recent quantum chemical calculations support the initial binding of molecular oxygen to the iron center forming an epoxide-like structure upon oxygen insertion into the C–C bond.[8]

In previous studies several functional models have been synthesized in order to gain insight into the mechanism of catechol

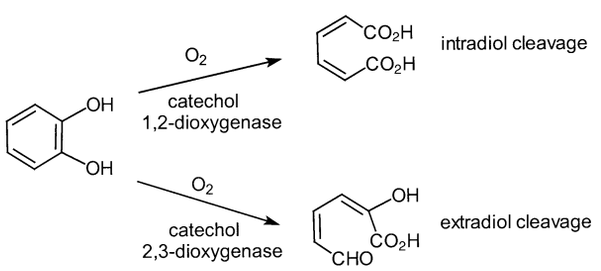

Fig. 1 Modes of catechol cleavage catalyzed by catechol 1,2-dioxygenases (intradiol cleavage) and catechol 2,3-dioxygenases (extradiol cleavage).

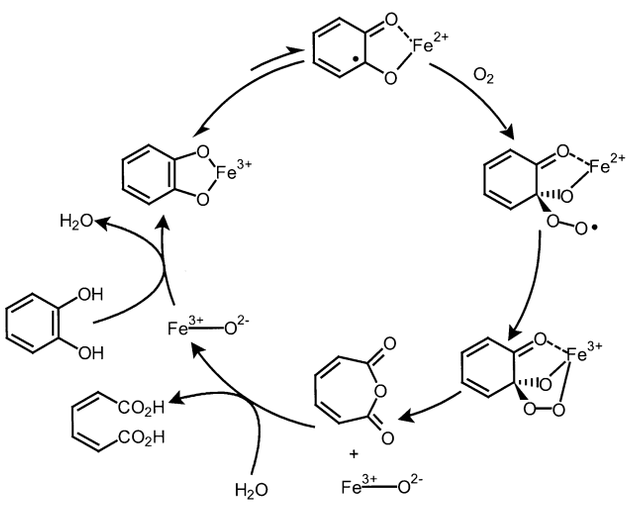

Fig. 2 Proposed substrate activation mechanism of catechol 1,2-dioxygenases.

† This paper is dedicated to Professor Dieter Sellmann on the occasion of his 60th birthday.

 DOI: 10.1039/b0085111

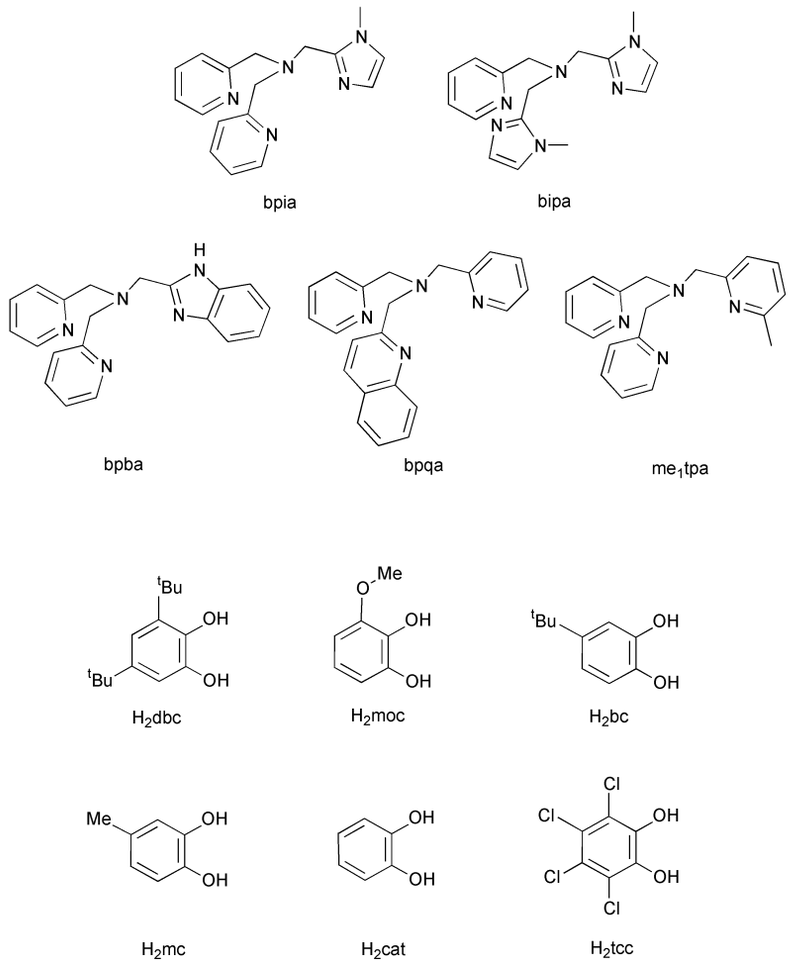

Fig. 3 Structures of the tripodal tetradentate ligands and catechol derivatives used in this work.

cleavage.[9–12] Especially tetradentate tripodal ligands have shown considerable abilities to regulate the properties of model complexes,[6,9,13–16] indicating that the dioxygenase activity strongly depends on the nature of the ligand set. With such tripodal ligands distorted coordination spheres are formed similar to the steric situation in the metalloproteins. Two *cis* coordination sites, essential for substrate binding, remain unoccupied. Model compounds synthesized by Que and Palaniandavar and co-workers consist of tripodal ligands with pyridine, carboxylate, benzimidazole, or phenolate moieties and 3,5-di-*tert*-butylcatechol (H_2dbc) as substrate analogue.[6,9,16] The advantages of this substrate are the relatively high stability of the main cleavage product (3,5-di-*tert*-butyl-1-oxacyclohepta-3,5-diene-2,7-dione) and the fast reaction of the catecholate complexes with dioxygen.[6,9,17,18] Little work has been devoted to the oxygenation of other catechols and their structural modeling.[19,20]

There are only a few reports on structural and functional model complexes for catechol 1,2-dioxygenase enzyme–substrate complexes.[6,9,10,12,19,21] These iron(III) catecholate complexes are of considerable interest as such species are formed in the first step of the reaction mechanism (Fig. 2).

Here we describe the first model compounds for catechol 1,2-dioxygenases with the inhibitor substrate tetrachlorocatechol (H_2tcc; yielding air stable complexes) and various tripodal ligands (Fig. 3) that exclusively provide nitrogen donors. In this series of tripodal ligands one donor moiety was changed systematically. The steric and electronic influence of the nitrogen-donor ligand set and of various catechols (Fig. 3) on the biomimetic and catalytic catechol 1,2-dioxygenase activity is probed with spectroscopic and functional investigations on *in situ* prepared iron(III) complexes.

Results and discussion

Syntheses

The synthesized ligands are derivatives of the exclusively pyridine containing tripodal ligand tpa (tris[(2-pyridyl)methyl]-amine). They selectively leave two *cis* oriented coordination sites at the iron(III) center unoccupied. A systematic ligand variation (Fig. 3) of one donor arm was achieved with methylimidazole (bpia: [(1-methylimidazol-2-yl)methyl]bis-[(2-pyridyl)methyl]amine), benzimidazole (bpba: [(benzimidazol-2-yl)methyl]bis[(2-pyridyl)methyl]amine), quinoline (bpqa: bis[(2-pyridyl)methyl][(2-quinolyl)methyl]amine), and methylpyridine (me_1tpa: [(6-methyl-2-pyridyl)methyl]bis[(2-pyridyl)-methyl]amine). For reactivity studies complexes of the ligand bipa (bis[(1-methylimidazol-2-yl)methyl][(2-pyridyl)methyl]-amine) were also synthesized (Fig. 3). In this ligand one pyridine and two methylimidazole moieties are attached to the central tertiary amine. All ligands synthesized provide N_4-donor sets. Such donor groups mimic the metal coordinating side chains of amino acids (histidine) in many enzymes.

The tripodal ligands bpia, me_1tpa, bpqa and bipa were prepared by slightly modified procedures described in the literature.[13,22–24] The novel benzimidazole containing ligand bpba was prepared *via* [(2-benzimidazolyl)methyl]amine and subsequent reaction with two equivalents of 2-pyridylmethyl chloride hydrochloride. The novel iron(III) catecholate complexes $[Fe(bpia)(tcc)]ClO_4$ **1**, $[Fe(bpba)(tcc)]ClO_4 \cdot (CH_3)_2CO$ **2**, $[Fe(bpqa)(tcc)]ClO_4 \cdot CH_3CH_2OH$ **3**, and $[Fe(me_1tpa)(tcc)]NO_3$ **4** were synthesized and crystallized by similar synthetic routes from iron(III) perchlorate and nitrate, respectively, and the corresponding tetradentate ligand. Upon addition of tetrachlorocatechol and treatment with two equivalents of piper-

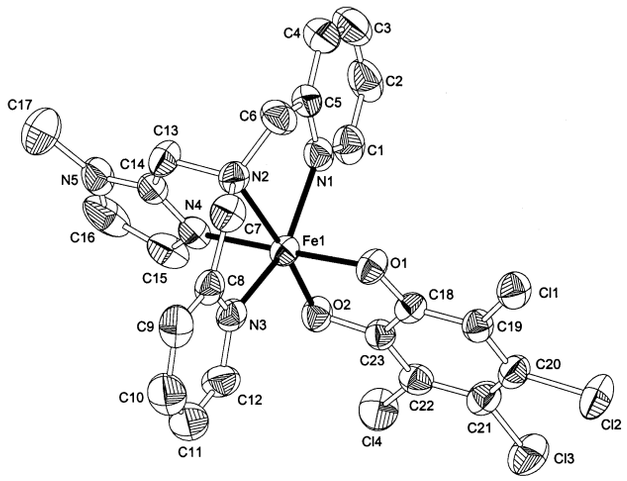

Fig. 4 Structure of the complex cation in $[Fe(bpia)(tcc)]ClO_4$ **1** with thermal ellipsoids (50% probability); hydrogen atoms omitted for clarity.

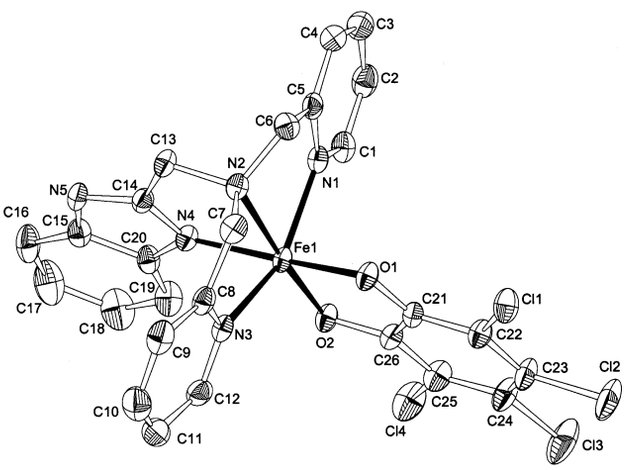

Fig. 5 Structure of the complex cation in $[Fe(bpba)(tcc)]ClO_4 \cdot (CH_3)_2CO$ **2**. Details as in Fig. 4.

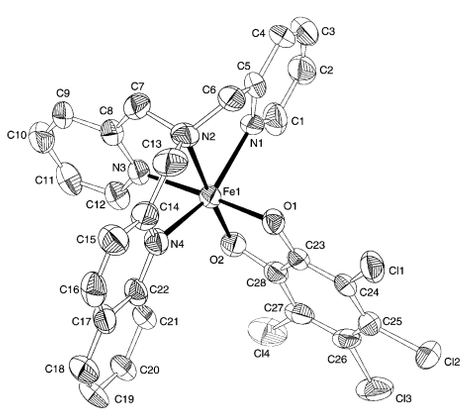

Fig. 6 Structure of the complex cation in $[Fe(bpqa)(tcc)]ClO_4 \cdot CH_3CH_2OH$ **3**. Details as in Fig. 4.

idine the complex solutions change from yellow-red to dark purple due to the formation of catecholate to iron(III) charge transfer transitions between 500 and 1000 nm. Single crystals suitable for X-ray crystallography were obtained upon slow cooling and standing of the reaction mixtures. The structures of the complex cations in **1**–**4** are shown as ellipsoid plots in Figs. 4–7. Table 1 gives a comparison of selected bond lengths and angles for the four structures. In Table 2 a comparison of selected bond lengths and angles for the determined structures and other well documented six-coordinate iron(III) catecholate complexes with N_4-donor ligands is listed.

Table 1 Selected bond lengths [Å] and angles [°] in complexes **1**–**4**

	1	**2**	**3**	**4**
Fe(1)–O(1)	1.948(3)	1.9612(17)	1.950(5)	1.938(5)
Fe(1)–O(2)	1.919(3)	1.8970(18)	1.911(6)	1.917(7)
Fe(1)–N(1)	2.120(4)	2.117(2)	2.190(6)	2.146(6)
Fe(1)–N(2)	2.246(4)	2.208(2)	2.160(6)	2.180(7)
Fe(1)–N(3)	2.126(4)	2.139(2)	2.128(5)	2.132(6)
Fe(1)–N(4)	2.081(4)	2.083(2)	2.153(6)	2.171(7)
O(1)–C	1.333(5)	1.325(3)	1.371(8)	1.304(9)
O(2)–C	1.330(5)	1.334(3)	1.326(8)	1.340(9)
O(1)–Fe(1)–O(2)	84.7(1)	85.19(8)	85.1(2)	83.9(2)
O(1)–Fe(1)–N(1)	89.8(1)	92.81(8)	91.8(2)	95.0(2)
O(1)–Fe(1)–N(2)	102.5(1)	92.92(8)	98.4(2)	106.4(2)
O(1)–Fe(1)–N(3)	93.3(1)	91.02(8)	177.0(2)	171.3(3)
O(1)–Fe(1)–N(4)	176.0(1)	173.42(7)	92.6(2)	91.2(2)
O(2)–Fe(1)–N(1)	104.8(2)	99.62(8)	98.2(2)	94.4(3)
O(2)–Fe(1)–N(2)	172.8(1)	176.04(7)	173.3(2)	166.6(2)
O(2)–Fe(1)–N(3)	102.8(2)	106.47(8)	95.3(2)	89.8(2)
O(2)–Fe(1)–N(4)	92.8(1)	101.15(8)	106.8(3)	111.7(3)
N(1)–Fe(1)–N(2)	76.2(2)	76.97(8)	76.0(2)	76.4(3)
N(1)–Fe(1)–N(3)	152.4(2)	153.86(8)	91.1(2)	91.6(2)
N(1)–Fe(1)–N(4)	87.9(1)	87.89(8)	154.9(2)	153.7(3)
N(2)–Fe(1)–N(3)	76.3(1)	77.01(8)	81.5(2)	80.8(2)
N(2)–Fe(1)–N(4)	80.2(1)	80.86(8)	78.9(3)	77.4(3)
N(3)–Fe(1)–N(4)	90.2(1)	85.52(8)	84.4(2)	85.4(2)

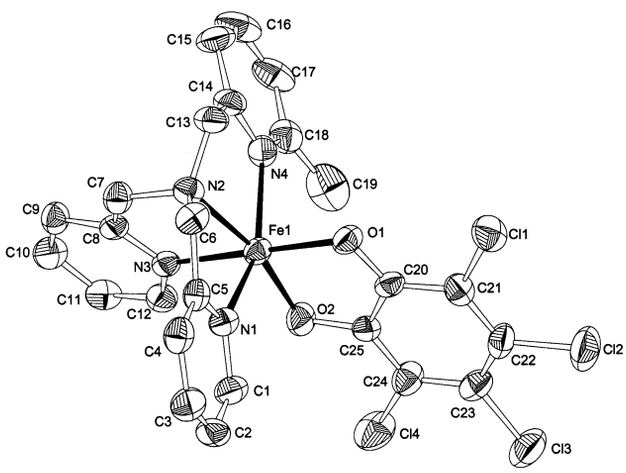

Fig. 7 Structure of the complex cation in $[Fe(me_1tpa)(tcc)]NO_3$ **4**. Details as in Fig. 4.

Crystal structures of complexes 1–4

The structure analyses of the four complexes show very similar features. The iron(III) cores are in distorted octahedral coordination spheres involving the N_4O_2-donor sets of the ligands and tetrachlorocatecholate.

The Fe–N bond lengths to the aromatic heterocycles pyridine, imidazole, and quinoline (Fe(1)–N(1)/N(3)/N(4)) are smaller than to the tertiary amine donors (Fe(1)–N(2)) due to their different π-donating properties. As a result of the extended π-molecular orbitals and electrostatic effects the coordinated catecholate units form the shortest bond lengths (Fe(1)–O(1)/O(2)). The *trans* effect of the weakly bound tertiary amine nitrogen donor causes slightly decreased bond lengths of the oxygen donors in *trans* position (O(2)). However, the very small differences in the C–O ($\Delta_{max} = 0.045$ Å) and Fe–O ($\Delta_{max} = 0.064$ Å) bond lengths within each complex clearly indicate that the ligand coordinates with its two phenolate donors (tetrachlorocatecholate) rather than with a phenolate and a quinone donor (tetrachlorosemiquinone). The slightly differing Fe–O bond lengths are caused by the asymmetry of the $[Fe(L)]^{3+}$ complex. The use of complexes with a higher symmetry will lead to identical Fe–O bond lengths (Table 2).[12] This is also supported by the more or less equal C–C lengths within

Table 2 Comparison of selected structural and spectroscopic data

	Fe–O/Å	O(2)–Fe(1)–N(4)/°	λ/nm (ε/M^{-1} cm^{-1})	$E_{1/2}$ [a]/mV	References
[Fe(bpia)(tcc)]ClO_4 **1**	1.948(3) 1.919(3)	92.8	529 (2080), 729 (3100)	+345	This work
[Fe(bpba)(tcc)]ClO_4·$(CH_3)_2CO$ **2**	1.961(2) 1.897(2)	101.2	532 (1817), 678 (2041)	+425	This work
[Fe(bpqa)(tcc)]ClO_4·CH_3CH_2OH **3**	1.950(5) 1.911(6)	106.8	590 (1989)	+466	This work
[Fe(me_1tpa)(tcc)]NO_3 **4**	1.938(5) 1.917(7)	111.7	577 (2746), 743 (3199)	+464	This work
$[Fe(bipa)]^{3+}$	—	—	—	+315	This work
[Fe(tpa)(dbc)]BPh_4·CH_3CN	1.917(3) 1.898(2)	—	568, 883	—	9
[Fe(N_4Me_2)(cat)]BPh_4	1.915(3) 1.903(3)	—	501, 734	—	10
[Fe(bispicme$_2$en)(dbc)]BPh_4	1.914(2) 1.914(4)	—	550 (1250), 925 (1850)	—	12

Abbreviations: bispicme$_2$en = *N*,*N*′-dimethyl-*N*,*N*′-bis(2-pyridylmethyl)ethane-1,2-diamine; H_2cat = pyrocatechol; N_4Me_2 = *N*,*N*′-dimethyl-2,11-diaza[3.3](2,6)-pyridinophane. [a] Values reported for the *in situ* prepared $[Fe(L)Cl_2]^+$ complexes.

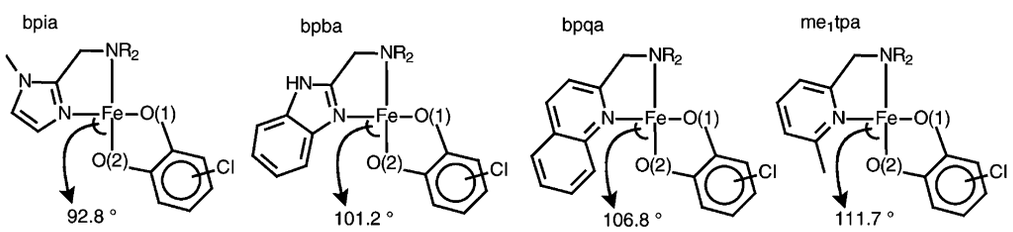

Fig. 8 The influence of the third ligand arm on the angle O(2)–Fe(1)–N(4) displaying the shielding of the iron center.

the tetrachlorocatecholate ligands of **1** – **4** which are consistent with an aromatic ring system with delocalized π bonds. For semiquinone species more pronounced differences in C–C bond lengths would be expected.[25] The semiquinone radical species are essential for a reaction with dioxygen.

Owing to the limiting bite of the ligands the *cis* angles (N(2)–Fe(1)–N(1)/N(3)/N(4)) are small. This is a typical structural feature in complexes of tripodal tetradentate ligands.

In compounds **2** and **3** the counter ions are stabilized by hydrogen bonds from the NH function of the benzimidazole group and of the OH group of one ethanol solvate molecule, respectively.

All four complexes described above differ mainly in the aromatic donor set of one ligand arm. The influence of this ligand arm can be described by the angle O(2)–Fe(1)–N(4) as depicted in Fig. 8 and Table 2. This angle correlates with an increasing steric demand of the ligand residue. Accordingly, the largest value was determined for complex **4** with the ligand me_1tpa, caused by one methyl substituent.

Spectroscopic characterization of complexes 1–4

The different Lewis acidities of the iron(III) center, influenced by the tripodal ligands, are reflected in the position of the two tetrachlorocatecholate to iron(III) charge transfer bands (located in the visible region of the spectra at around 500–1000 nm; Table 2).[6,9] With increasing Lewis acidic character the higher energy absorption bands are shifted to lower energies (*i.e.* higher wavelengths) in the order **1** < **2** < **4**. For complex **3** there was found to be only one broad CT absorption band at 590 nm. The reason for this, *i.e.* veiling of one band by other more intense bands, merging of the two bands, or a different binding mode of tcc in solution, remains unclear. Therefore, the iron core in **4** shows the highest electron accepting character. More strongly electron donating catechols (*e.g.* in [Fe(tpa)-(dbc)]BPh_4 or [Fe(N_4Me_2)(cat)]ClO_4) yield complexes with UV/Vis bands at higher wavelengths (Table 2).

Typical bands of the ligands are found in the vibrational spectra of the complexes. A characteristic shift of CN bands is observed due to coordination of the ligands to the iron(III) ion. Bands at high wavenumbers are found due to incorporation of solvent into the crystal.

The cyclic voltammograms of complexes **1**–**4** are rather complicated. Both the iron center and the catecholate ligand are redox active. The redox chemistry at the iron center is affected by the instability of the electrochemically produced iron(III) semiquinone species.[6,9] Such species disintegrate yielding iron(II) complexes and quinone when working with Lewis acidic iron cores, resulting in irreversible and ill defined redox features.[6,9] On the basis of these cyclic voltammograms a complete assignment of redox processes was not possible. Therefore, *in situ* prepared iron chloro complexes and the catechols were examined separately electrochemically.

In order to determine the spin-state properties of the metal ions we performed temperature-dependent magnetic susceptibility measurements on powdered samples of **1**–**4**. All four complexes show the expected paramagnetic behavior of mononuclear high-spin iron(III). They follow the Curie–Weiss law ($\chi_m = C/(T - \theta)$) in the temperature range 40–300 K. The magnetic moments for **1**, **3** and **4** were measured to be 5.7, 6.0 and 6.0μ_B indicative for high-spin iron(III) ions with $S = 5/2$ (expected spin only moment $\mu_{eff} = 5.9\mu_B$).[26] Usually values in the range of 5.7–6.2μ_B are found.[26] For **2** a very low moment of 4.8μ_B was measured. This value is obviously not indicative of a high-spin $S = 5/2$ center but is also really too high to be considered as a pure $S = 3/2$ intermediate spin or $S = 1/2$ low-spin system. So far there are no hints of a quantum mechanical mixing of two states that can occur to create a new, discrete spin-admixed ground state that has elements of two spin states.[26,27] The system is under further spectroscopic investigation.

Investigation of the *in situ* prepared iron complexes

The iron(III) complexes with general formula $[Fe(L)]^{3+}$ (L = tripodal ligand) were prepared from iron(III) perchlorate and studied in solution using UV/Vis spectroscopy. Ligand metallation (bpia; Fig. 9) is accompanied by distinct spectral changes

Table 3 Redox potentials of the catechols (Fig. 3) and the UV/Vis spectroscopic and kinetic data of the [Fe(bpba)(catecholate)]$^+$ complexes for the reaction with air (T = 298 K)

Catechol	$E_{1/2}$/mV (H_2cat–Q)	E_C/mV ($H^+_{cat}-\frac{1}{2}H_2$)	λ/nm (ε/M^{-1} cm^{-1})	k/M^{-1} s^{-1}
H_2dbc	−222	−885	569 (1443), 877 (2095)	2.9
H_2moc	−152	−973	656, sh (1471), 827 (1653)	2.4
H_2bc	−142	−912	525 (1345), 824 (1836)	0.76
H_2mc	−123	−927	520 (1283), 835 (1862)	0.91
H_2cat	−46	−922	503 (1201), 785 (1665)	0.031
H_2tcc	+312	−855	532 (1817), 678 (2041)	$<10^{-5}$

Abbreviations: H_2bc = 4-*tert*-butylcatechol; H_2mc = 4-methylcatechol; H_2moc = 3-methoxycatechol.

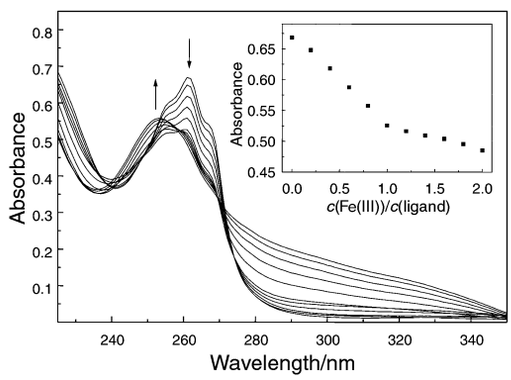

Fig. 9 Titration of bpia (c = 0.1 mmol L^{-1}) with 0.2 equivalent portions of $Fe(ClO_4)_3 \cdot 9H_2O$ solution in methanol at 295 K followed by UV/Vis spectroscopy. Inset: plot of absorbance *vs.* $c(Fe^{III})/c$(bpia) at 261 nm.

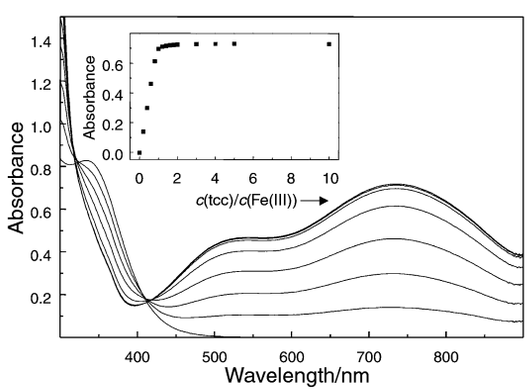

Fig. 10 Titration of [Fe(bpia)]$^{3+}$ (c = 0.25 mmol L^{-1}) and piperidine (c = 0.5 mmol L^{-1}) with 0.2 equivalent portions of tetrachlorocatecholate monohydrate solution in methanol at 295 K followed by UV/Vis spectroscopy. Inset: plot of absorbance *vs.* c(tcc)/$c(Fe^{III})$ at 734 nm.

of the ligand bands with an isosbestic point at 274 nm in the ratio range of 0 : 1 to 1 : 1. The isosbestic point disappears at higher amounts of iron(III). This implies that the tripodal ligands exclusively coordinate a single iron(III) ion. In a similar manner, the [Fe(L)]$^{3+}$ complexes (L = tripodal ligand) were titrated with catecholate (tcc). The original spectrum of the [Fe(bpia)]$^{3+}$ complex (Fig. 10) changes dramatically upon addition of tcc due to the formation of two ligand to metal charge transfer bands in the visible region. The intensities of the charge transfer bands increase with increasing catecholate to complex ratio. These spectral changes were observed until the ratio of concentration of the ligand and Fe^{3+} was 1 : 1 (inset Fig. 10). At higher catechol concentrations the spectra remained essentially unchanged. These experiments underscore the assumption that the *in situ* complex syntheses exclusively yield mononuclear catecholate species with general formula [Fe(L)(cat)]$^+$ (L = tripodal ligand; cat = catecholate). The UV/Vis spectra of the structurally characterized complexes and the *in situ* prepared complexes are identical. It can therefore be excluded that simple iron(III) catecholate complexes are formed upon demetallation of the tripodal ligand.

Unambiguous assignment of redox features was not possible in the cyclic voltammograms of the crystallized iron(III)–tcc complexes **1**–**4**. Thus, the electrochemical features of the *in situ* formed iron(III) chloro complexes of type [Fe(L)Cl_2]$^+$ using iron(III) chloride were investigated with cyclic voltammetry. All of the complexes exhibit at positive potentials a coupled pair of redox waves that are assigned to the iron(III)–iron(II) couple (Table 2). The cyclic voltammograms of structurally characterized iron(III) chloro complexes show similar features.[13,14,16] The order of the complex series [Fe(bpia)]$^{3+}$ < [Fe(bpba)]$^{3+}$ < [Fe(me_1tpa)]$^{3+}$ < [Fe(bpqa)]$^{3+}$ indicates increasing Fe^{3+}–Fe^{2+} redox potential of the complexes caused by the electron accepting character of the tripodal ligand. The high redox potentials of the me_1tpa and bpqa complexes are the result of the extended aromatic systems of one donor moiety. For comparison purposes we also investigated the electrochemical properties of the catechol derivatives. The cyclic voltammograms of the six catechols exhibit one reduction peak between −850 and −980 mV with no observable anodic peak coupled to it (Table 3). This feature can be associated with the reduction of catechol protons.[28] At higher voltages (−370 to 350 mV) all catechols show an additional cathodic as well as an anodic wave (Table 3). These peaks correspond to a two-electron process of the couple H_2cat–Q (Q = quinone).[28,29] In the series H_2dbc, H_2moc, H_2bc, H_2mc, H_2cat, and H_2tcc the redox potentials increase due to the decreasing electron donating potential of the catechol substituents and the resulting decrease in Lewis basicity of the catechols. The redox potentials of the various substrates are listed in Table 3.

Catechol cleavage of iron(III) complexes

After the characterization of the *in situ* prepared complexes their catechol 1,2-dioxygenase activity was examined. This reactivity and the positions of the two ligand-to-metal charge transfer bands which are formed upon addition of catechol to a solution of [Fe(L)]$^{3+}$ strongly depend on the amount of base added for deprotonation of the catechol. The fastest reactions take place when approximately 2.0 to 2.5 equivalents of base (piperidine) are added and the UV/Vis bands are shifted to a minimum of energy. At higher concentrations of base the reaction rates decrease and a shift to lower wavelengths is observed due to competitive coordination of base to the iron center. Our experiments were carried out for each complex at the highest possible reaction rate (details are given in the Experimental section; Table 7). For comparable kinetic results the exact amount of base was determined before each reaction.

As an example, the progress of the reaction of the bpba complex with dbc and dioxygen is shown in Fig. 11. The inset displays the logarithm of the absorbance *versus* time. Upon addition of catechol the reaction solution changes from red to dark purple as a result of catechol binding (the resulting bands in the spectrum can be assigned to moderately intense

Table 4 UV/Vis spectroscopic and kinetic data of $[Fe(L)]^{3+}$ complexes for the reaction with the substrate H_2moc in the presence of air (T = 298 K)

Complex	λ/nm (ε/M^{-1} cm^{-1})	k/M^{-1} s^{-1} (Δ_{max}=15%)
$[Fe(bpia)(moc)]^+$	644, sh (1490), 818 (1745)	5.3
$[Fe(bpba)(moc)]^+$	656, sh (1471), 827 (1653)	2.4
$[Fe(bipa)(moc)]^+$	627, sh (1792), 797 (2113)	0.47
$[Fe(me_1tpa)(moc)]^+$	681, sh (1571), 866 (1686)	0.093
$[Fe(bpqa)(moc)]^+$	688, sh (1902), 869 (2052)	0.017

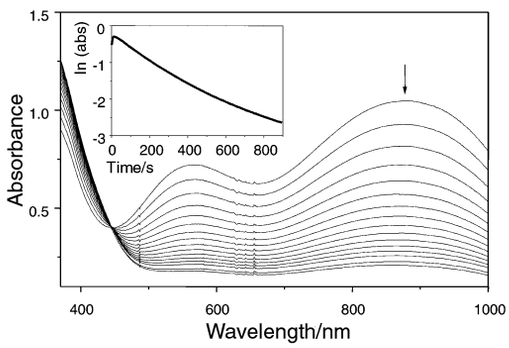

Fig. 11 Progress of the reaction of $[Fe(bpba)(dbc)]^+$ with air (measurement interval: 30 s). Inset: plot of ln(abs) *vs.* time for the $[Fe(bpba)(dbc)]^+$ reaction at 298 K.

catecholate-to-iron(III) LMCT transitions in the visible region). The disintegration of the complex is indicated by the disappearance of the purple color. Finally, the color of the catecholate free iron complex is observed at the end of each experiment.

The reactions of all $[Fe(L)]^{3+}$ complexes with any catechol (1 : 1 ratio for Fe : catechol) and O_2 show pseudo-first-order kinetics due to the excess of dioxygen.[6,10,13,14,19] The pseudo-first-order constants were determined by linear fitting of the logarithmic plot (inset in Fig. 11). The second-order constants were calculated with $[O_2] = 2.12 \times 10^{-3}$ M at 298 K in methanol.[13,14,30] Representative results of the UV/Vis spectroscopic and kinetic analyses for the reactions in the presence of air are given in Tables 3 and 4. Under our conditions, no catechol cleavage activity was found for iron(III) ions alone.

The reaction rates observed by varying the catechol while maintaining one iron complex show a direct dependence on the redox potential of the catechol derivative. The energies of the CT bands in the UV/Vis spectra show inverse correlations. Fig. 12 demonstrates this relation in wavenumber/redox potential and reaction rate constant/redox potential diagrams for one representative iron complex. By far the most unreactive catechol is H_2tcc as a result of its relatively high redox potential. Accordingly, the LMCT bands of the tcc containing complex occur at the lowest wavelengths observed within this series. Iron tcc complexes are so stable that they can be handled in an oxygen atmosphere. In contrast, H_2dbc and H_2moc are the most reactive catechols as a result of their electron donating groups. The LMCT bands of their complexes are found at high wavelengths. The dbc complexes with the ligands me_1tpa and bpqa have iron cores with the highest Lewis acidities (Table 2) and the catechol with the highest Lewis basicity (Table 3). Consequently, the LMCT bands are observed at low energies. This is consistent with the UV/Vis spectroscopic features of the structurally characterized complexes (Table 2) with the weakly electron donating catecholate tcc. A similar relationship for phenolate bearing tripodal ligand systems is reported by Viswanathan *et al.*[16] The catecholate-to-iron(III) LMCT bands are found at higher energies (lower wavelengths). This is due to the higher electron donor character of the phenolate moieties.

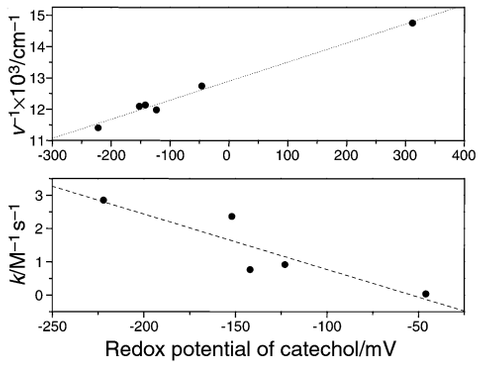

Fig. 12 Top: correlation of LMCT energies and redox potential of the catechol. Bottom: relation between the reaction rate constant (k) and the redox potential of the catechol. Both series were recorded for complexes of general formula $[Fe(bpba)(catecholate)]^+$.

On the other hand, the variation of the tripodal ligand in the $[Fe(L)]^{3+}$ complexes during the dioxygenation reaction shows a more complicated behavior. The spectroscopic investigation of the complexes suggests an order of reactivity according to the Lewis acidity of the iron center (Table 2). Instead, the complex reactivity decreases in the series bpia > bpba > bipa > me_1tpa > bpqa. Small reaction rate constants are observed for iron complexes with a high redox potential and with CT bands at low energies. The rate constant of the iron complexes $[Fe(L)]^{3+}$ for the reaction with one chosen substrate (H_2moc; Table 4) drops by two orders of magnitude from 5.3 (bpia) to 0.017 (bpqa). This is a result of the different steric requirements of the ligand moieties. A very reactive complex always contains a sterically low demanding ligand. Under such conditions the iron ion is easily accessible to both the catechol and oxygen. The values of the O(2)–Fe(1)–N(4) angles determined by structure analyses explain this finding. The complex with the relatively small ligand bpia has a smaller angle and, accordingly, the highest reactivity. On the other hand, larger substituents attached to the tertiary amine (*e.g.* in me_1tpa or bpqa) yield slowly reacting complexes due to the interference of the ligand substituents with the substrate and oxidant (large O(2)–Fe(1)–N(4) angle). Nevertheless, the Lewis acidity of the iron center in the me_1tpa complex is high; bipa is the smallest ligand but the Lewis acidity of the iron(III) core is comparably low due to the ligand's two imidazole residues.

These results support the mechanism of Que and co-workers proposing a substrate activation.[1,3,4,6–9] With a lower electron accepting character (lower redox potential) of the complex and a lower electron donating character (higher redox potential) of the substrate, respectively, the semiquinone character of the catechol is decreased. Under these circumstances the attack of dioxygen is disfavored. On the other hand, an electron rich catechol with a low redox potential leads to more contribution of the Fe^{II}–semiquinone species and, thus, to faster reaction rates. A highly reactive catechol 1,2-dioxygenase modeling system always consists of an electron accepting iron(III) complex and of an electron donating catechol.

All systems investigated are highly reactive towards dioxygen yielding the desired product of intradiol cleavage. In the stoichiometric reactions neither the products of the extradiol cleavage nor the products of the simple oxidation reaction, quinones (**VII** in Fig. 13), could be isolated as by-products. In previous studies on reactions with other iron(III) dbc complexes **I** was identified as the main oxidation product.[9,17,18] Mialane *et al.* observed as the major product 3,5-di-*tert*-butyl-5-(carboxymethyl)-2-furanone (**IV** with $R^1 = R^2 =$ *tert*-butyl) which was due to longer reaction times.[12] We found that the product formation depends on the catechol used. With H_2dbc and H_2moc, the catechols with the lowest redox potentials and, therefore, the highest reactivities, stable 3,5-di-*tert*-butylmuconic acid anhydride (**I**) and 2-methoxymuconic acid

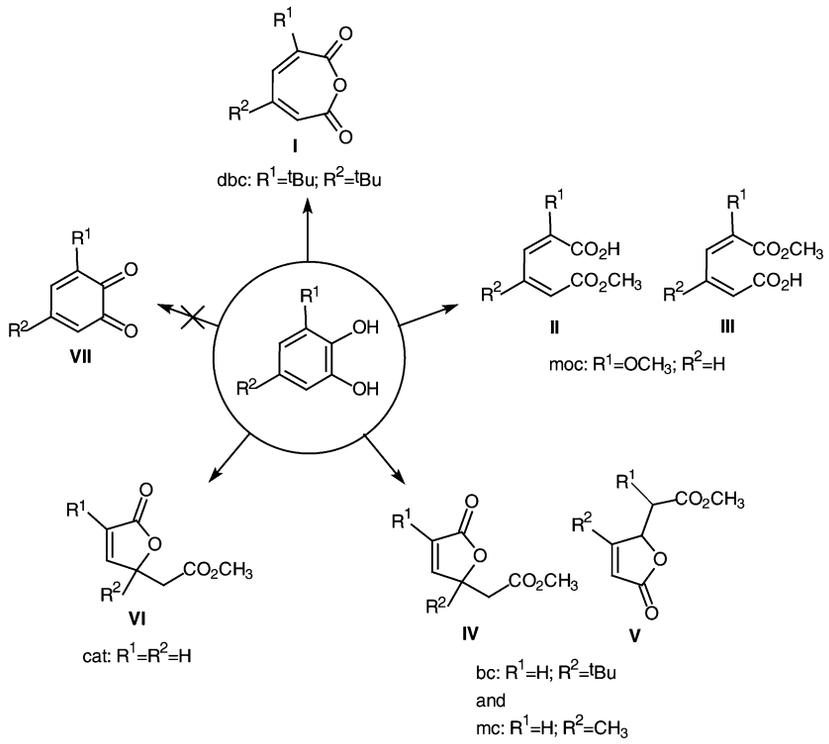

Fig. 13 Products of catechol cleavage mediated by iron(III) complexes with 3,5-di-*tert*-butylcatechol, 3-methoxycatechol, 4-*tert*-butylcatechol, 4-methylcatechol and pyrocatechol as substrates.

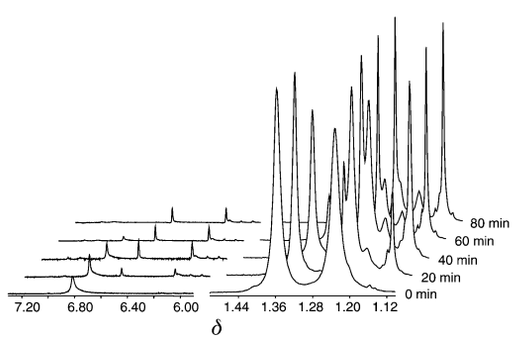

Fig. 14 Progress of the catalytic reaction of $[Fe(bpba)]^{3+}$ with 10 equivalent H_2dbc and air in the presence of 2 equivalents of piperidine at 295 K followed by ^{1}H NMR spectroscopy.

monomethyl ester (**II**, **III**), respectively, are formed. The catechols with lower reactivities (H_2bc, H_2mc, and H_2cat) yield furanones (**IV**, **V**, **VI**) as oxygenated products. These furanones are formed upon methanolysis of the unstable muconic acid anhydride as the Markovnikov product of γ-lactonization. Owing to its extremely low reactivity no products could be isolated using H_2tcc as a substrate.

These systems model the functional and structural behavior of catechol 1,2-dioxygenases. The complexes with the highest reactivities show catalytic cleavage of the substrates H_2dbc and H_2moc. In the presence of 0.1 equivalent catalyst H_2dbc and H_2moc are converted rapidly (over 40–160 min) and efficiently into the dioxygenated products. The undesired products of the simple oxidation (**VII** in Fig. 13) were formed only in very small yields (<6%). The reactions (with 0.1 and 0.01 equivalent of complex) were followed using ^{1}H NMR spectroscopy and the yields could be determined by integration of the product signals in the range between δ 6 and 7 with CH_3NO_2 as internal standard. As an example, the trace of the reaction of $[Fe(bpba)]^{3+}$ with H_2dbc is shown in Fig. 14. In the beginning of the reaction broad signals of the substrate are observed due to the paramagnetic behavior of the mononuclear catalyst. Upon dioxygenation the peaks of 3,5-di-*tert*-butylmuconic acid anhydride appear and the width of the signals decreases. This is

Table 5 Yields (%) of the catalytically cleaved highly reactive catechols H_2dbc and H_2moc (Δ_{max}=11%)

Complex	10 equivalents H_2dbc	100 equivalents H_2dbc	10 equivalents H_2moc
$[Fe(bpia)]^{3+}$	84	68	74
$[Fe(bpba)]^{3+}$	69	65	74
$[Fe(bipa)]^{3+}$	68	30	46

the result of the formation of an antiferromagnetically coupled dinuclear complex.[10,13,19,31] The best performance was observed for the complex $[Fe(bpia)]^{3+}$ with a turnover number of 68 for the reaction with 100 equivalents of H_2dbc. 1% of the catalyst converts H_2dbc into the oxygenated product over 0.5 (bpia) to 3 days (bipa) (Table 5). According to their reactivity the catalytic activities of the complexes decrease in the series $[Fe(bpia)]^{3+} > [Fe(bpba)]^{3+} > [Fe(bipa)]^{3+}$. This result is also consistent with the different Lewis acidities of the iron cores and the different steric demands of the ligands revealed in the crystal structures. Therefore, small aromatic nitrogen-donor moieties with electron accepting character improve the catalytic activity (higher yield and a faster reaction) of iron(III) complexes with tripodal ligands in contrast to the behavior of phenolate bearing tripodal ligands.[16] All product yields of the oxidative cleavage of H_2dbc and H_2moc are listed in Table 5.

Conclusion

The synthesized mononuclear iron(III) complexes with tripodal N_4-donor ligands and catecholate are structural and functional model compounds for catechol 1,2-dioxygenase enzyme–substrate adducts. The ligand groups imidazole, pyridine, and quinoline have different steric demands clearly influencing the shielding of the iron(III) center.

With the tripodal tetradentate ligands only mononuclear complexes with one bound substrate molecule are formed in solution. All *in situ* prepared complexes are highly reactive with respect to aerial oxidation of various catechols to their corresponding cleavage products. A clear relationship between the

electrochemical properties of the catechols, the UV/Vis absorption features and the reaction rate constant is observed. Accordingly, a catechol with a high redox potential (H_2tcc) results in low reaction rate constants and LMCT transitions at low wavelengths. Also a correlation between the steric demand of the ligands and the reactivity of the complexes is found. A large angle O(2)–Fe(1)–N(4) causes low reaction rate constants. Therefore, a highly reactive complex requires a ligand that induces a high Lewis acidity at the iron(III) center and that consists of small coordinating groups. An electron transfer mediated substrate activation mechanism as proposed by Que and co-workers can be supported.[1,3,4,6–9]

The complexes with the highest reactivities show catalytic behavior with respect to the oxidative cleavage of H_2dbc and H_2moc. In ^{1}H NMR experiments product yields up to 84% could be obtained depending on the catechol and on the catalyst, respectively. The catalytic activities strongly depend on (a) the reactivity of the complex and (b) the reactivity of the substrate. Both are influenced by the steric demands and the Lewis acidities of the iron complex and the Lewis basicities of the substrate, respectively. Small ligand moieties cause high reactivities. Under these conditions the iron complex is more open to approach of both the catechol as well as oxygen. Additionally, the small imidazole moiety supports a rapid replacement of the oxygenated product.

Experimental

Physical measurements

^{1}H and ^{13}C NMR spectra were recorded on a Bruker WH 300 instrument. The experiments on the catalytic cleavage of catechols were performed at 303 K on a Bruker AM 360-FT-NMR spectrometer (360 MHz). Elemental analyses were recorded on a Heraeus CHN-O-RAPID analyzer. Electronic spectra were recorded on a Hewlett Packard diode array spectrometer using quartz cuvettes ($d = 1$ cm; $T = 298$ K). Cyclic voltammetric experiments were performed on a BAS CV-50W instrument in acetonitrile (for complexes **1**–**4**; $c = 5 \times 10^{-4}$ mol L^{-1}) or in methanol (for the *in situ* synthesized $[Fe(L)Cl_2]^+$ complexes and for the catechols; for both $c = 5 \times 10^{-4}$ mol L^{-1}) with tetrabutylammonium perchlorate as supporting electrolyte ($c = 0.1$ mol L^{-1}). A three-electrode system with a glassy carbon working electrode, an Ag–AgCl–3 mol L^{-1} NaCl reference electrode, and a platinum wire as the auxiliary electrode was used. Under these conditions ferrocene has a potential of 370 mV. Mass spectra were measured on a Varian MAT 212 instrument, IR (in KBr) on a Bruker IF 113v spectrometer.

The starting materials were purchased from commercial sources (Fluka, Aldrich) and used as received unless otherwise noted.

Syntheses

[(1-Methylimidazol-2-yl)methyl]bis[(2-pyridyl)methyl]amine (bpia), [(6-methyl-2-pyridyl)methyl]bis[(2-pyridyl)methyl]amine (me$_1$tpa), bis[(2-pyridyl)methyl][(2-quinolyl)methyl]amine (bpqa), and bis[(1-methylimidazol-2-yl)methyl][(2-pyridyl)-methyl]amine (bipa). The precursor compounds bis[(2-pyridyl)methyl]amine, 2-chloromethyl-1-methylimidazole hydrochloride, and 2-(bromomethyl)quinoline for the ligand syntheses were prepared as described elsewhere.[13,32] The ligands bpia, me$_1$tpa, bpqa, and bipa were synthesized according to literature procedures.[13,22–24]

[(Benzimidazol-2-yl)methyl]amine. Similar to previously reported methods, glycine (33 g, 0.44 mol) and *ortho*-phenylenediamine (47.5 g, 0.44 mol) were dissolved in hydrochloric acid (200 mL, 7 M)[33] and refluxed with stirring for 72 hours. The product precipitated as its hydrochloride upon cooling to ambient temperature. The primary product was dissolved in water (200 mL) and the pH value adjusted to 8–9 with aqueous NH_3. Impurities were removed by extraction of the mixture with CH_2Cl_2 (2 × 50 mL). The product precipitated as colorless needles from the aqueous layer upon cooling to 4 °C. After drying with $CaCl_2$ *in vacuo*, it can be stored under Ar at room temperature. Yield: 22.6 g (0.154 mol, 35%). mp 44 °C. δ_H (300 MHz; D_2O; standard H_2O) 3.78 (s, 2H, CH_2), 7.14–7.17 (m, 2H, CH_{Bim}) and 7.41–7.44 (m, 2H, CH_{Bim}).

[(Benzimidazol-2-yl)methyl]bis[(2-pyridyl)methyl]amine (bpba). 2-(Chloromethyl)pyridine hydrochloride (3.9 g, 0.024 mol) was suspended in 40 mL of CH_2Cl_2 and cooled to 0 °C. [(Benzimidazol-2-yl)methyl]amine (1.04 g, 0.007 mol) suspended in 10 mL of CH_2Cl_2 was added, followed by dropwise addition of a solution of 5.6 g (0.055 mol) triethylamine in 20 mL of CH_2Cl_2. After stirring for 72 h at ambient temperature the organic mixture was extracted with water (50 ml) and dried with magnesium sulfate. The solvent was removed *in vacuo*. The resulting brown oil was extracted with hot CCl_4 and the product precipitated as colorless needles upon standing at −20 °C; bpba can be stored under argon under these conditions. Yield: 1.9 g (0.006 mol, 83%). mp 58 °C. δ_H (300 MHz; $CDCl_3$; standard $SiMe_4$) 3.93 (s, 4H, CH_{2Py}), 4.12 (s, 2H, CH_{2Bim}), 7.15–7.23 (m, 4H, CH_{Bim}), 7.31 (m, 2H, CH_{Py}), 7.57–7.64 (m, 4H, CH_{Py}) and 8.62 (m, 2H, CH_{Py}). δ_C (75 MHz; $CDCl_3$; standard $SiMe_4$) 45.9 (CH_{2Bim}), 59.9 (CH_{2Py}), 121.9 (C_{ar}), 122.5 (C_{ar}), 123.7 (C_{ar}), 136.8 (C_{ar}), 149.1 (C_{ar}), 153.4 (C_{ar}) and 158.5 (C_{ar}). MS (70 eV, 165 °C) *m*/*z* 329 (M^+, 5), 237 ($M - C_6H_6N$, 44), 198 (59), 132 (26), 131 ($C_8H_7N_2^+$, 41), 119 (11), 107 ($C_6H_7N_2^+$, 49), 93 ($C_6H_7N^+$, 100), 92 ($C_6H_6N^+$, 36), 78 ($C_5H_4N^+$, 11), 65 ($C_5H_6^+$, 27), 51 ($C_4H_3^+$, 8), 39 ($C_3H_3^+$, 13) and 28 ($C_2H_4^+$, 18%).

CAUTION: in general, perchlorate salts of metal complexes with organic ligands are potentially explosive. The shock sensitivities of the present perchlorate complexes are not proven, yet. Nevertheless, care is recommended while handling.

[Fe(bpia)(tcc)]ClO_4 1. $Fe(ClO_4)_3 \cdot 9H_2O$ (52 mg, 0.1 mmol), tetrachlorocatechol monohydrate (26 mg, 0.1 mmol), and bpia (29 mg, 0.1 mmol) were each dissolved in 2 mL of methanol–acetone (3 : 2) in separate vessels. The hot solutions were mixed and after addition of piperidine (20 μL) the reaction mixture was refluxed for a few seconds. Dark purple needles of complex **1** formed within a few days upon slow cooling and standing. Yield: 20 mg (0.029 mmol, 29%). mp decomp. >200 °C (Found: C, 39.6; H, 2.7; N, 9.8%. $C_{23}H_{19}Cl_5FeN_5O_6$ requires: C, 39.8; H, 2.8; N, 10.1%). λ_{max}/nm (ε/M^{-1} cm^{-1}) (methanol) 529 (2080) and 729 (3100).

[Fe(bpba)(tcc)]$ClO_4 \cdot (CH_3)_2CO$ 2. $Fe(ClO_4)_3 \cdot 9H_2O$ (52 mg, 0.1 mmol) was dissolved in acetone (2 mL). With stirring, solutions of the ligand bpba (33 mg, 0.1 mmol) and tetrachlorocatechol monohydrate (26 mg, 0.1 mmol), both in 2 mL acetone, were added. After addition of 27.5 μL NEt_3 the reaction mixture was refluxed for a few seconds and complex **2** precipitated as dark purple needles upon cooling and standing for several days. Yield: 32 mg (0.04 mmol, 39%). mp 278 °C (Found: C, 44.7; H, 3.4; N, 9.3%. $C_{29}H_{25}Cl_5FeN_5O_7$ requires: C, 44.2; H, 3.2; N, 8.9%). λ_{max}/nm (ε/M^{-1} cm^{-1}) (methanol) 532 (1817) and 678 (2041).

[Fe(bpqa)(tcc)]$ClO_4 \cdot CH_3CH_2OH$ 3. Solutions of $Fe(ClO_4)_3 \cdot 9H_2O$ (52 mg, 0.1 mmol), tetrachlorocatechol monohydrate (26 mg, 0.1 mmol), and bpqa (32 mg, 0.1 mmol) were each dissolved in 2 mL ethanol and combined. After addition of NEt_3 (27.5 μL) the reaction mixture was refluxed for a few seconds. Dark purple crystals precipitated upon slow cooling to ambient temperature and standing for several days. Yield: 55 mg (0.07 mmol, 65%). mp 242 °C (Found: C, 45.3; H, 3.3; N, 7.0%. $C_{30}H_{26}Cl_5FeN_4O_7$ requires: C, 45.7; H, 3.3; N, 7.1%). λ_{max}/nm (ε/M^{-1} cm^{-1}) (methanol) 590 (1989).

Table 6 Crystallographic data and experimental details

	1	**2**	**3**	**4**
Formula	$C_{23}H_{19}Cl_5FeN_5O_6$	$C_{29}H_{25}Cl_5FeN_5O_7$	$C_{30}H_{26}Cl_5FeN_4O_7$	$C_{25}H_{20}Cl_4FeN_5O_5$
M/g mol^{-1}	694.53	788.64	787.65	668.11
Crystal system	Monoclinic	Triclinic	Monoclinic	Triclinic
Space group	$P2_1/c$ (no. 14)	$P\bar{1}$ (no. 2)	$P2_1/n$ (no. 14)	$P\bar{1}$ (no. 2)
a/Å	9.120(2)	8.512(2)	9.553(2)	8.366(2)
b/Å	35.402(7)	9.754(2)	17.660(4)	9.211(2)
c/Å	8.666(2)	19.977(4)	20.095(4)	17.890(4)
α/°		88.17(3)		83.04(3)
β/°	92.93(3)	82.94(3)	102.13(3)	82.43(3)
γ/°		88.38(3)		89.25(3)
V/Å^3	2794.3(10)	1644.7(6)	3314.5(12)	1356.5(5)
Z	4	2	4	2
μ/mm^{-1}	1.066	0.919	0.911	0.997
T/K	213	150	173	213
Measured reflections	18772	7647	12000	8599
Unique reflections	5445	7152	5824	4442
Observed reflections [$I > 2\sigma(I)$]	4025	5633	3801	2319
Parameters	362	426	426	362
$R1$, $wR2$ [$I > 2\sigma(I)$]	0.0592, 0.1312	0.0416, 0.1173	0.0850, 0.2119	0.0756, 0.1576

[Fe(me$_1$tpa)(tcc)]NO$_3$ 4. Tetrachlorocatechol monohydrate (26 mg, 0.1 mmol) and me$_1$tpa (31 mg, 0.1 mmol), each dissolved in 2 mL ethanol, were added with stirring to a solution of $Fe(NO_3)_3 \cdot 9H_2O$ (41 mg, 0.1 mmol) in 2 mL ethanol. The resulting dark purple solution was treated with 27.5 μL of NEt_3 and refluxed for several seconds. Upon cooling and standing for a few days at ambient temperature dark purple needles were obtained. Yield: 27 mg (0.04 mmol, 44%). mp 233 °C (Found: C, 44.8; H, 3.1; N, 10.3%. $C_{25}H_{20}Cl_4FeN_5O_5$ requires: C, 44.9; H, 3.0; N, 10.5%). λ_{max}/nm (ε/M^{-1} cm^{-1}) (methanol) 577 (2746) and 743 (3199).

Single crystal X-ray diffraction

Intensity data of complexes **1** and **4** were collected on a STOE IPDS diffractometer (Mo-Kα, $\lambda = 0.71073$ Å, graphite monochromator), those for **2** and **3** on a Syntex P2$_1$ and a Siemens P3 four-cycle diffractometer, respectively (Mo-Kα, $\lambda = 0.71073$ Å, graphite monochromator), by using the ω-scan technique. The intensities of two reflections were monitored and no significant crystal deterioration was observed. Further data collection parameters are summarized in Table 6. The structure of **1** was solved by direct methods and those of **2**–**4** by Patterson syntheses (program SHELXS 97).[34] A series of full-matrix least-squares refinement cycles on F^2 (program SHELXL 97) followed by Fourier syntheses gave all remaining atoms.[35] The positions of the NH proton in **2** and the hydroxo proton of the ethanol solvate molecule in **3** were taken from the Fourier difference maps and refined with 1.5 times the U_{eq} value of the corresponding atom. All other hydrogen atoms were placed on calculated positions and constrained to ride on the atom to which they are attached. The isotropic thermal parameters for the methyl protons were refined with 1.5 times the U_{eq} value of the corresponding atom and for all other hydrogen atoms with 1.2 times U_{eq}. The non-hydrogen atoms were refined with anisotropic thermal parameters.

CCDC reference numbers 139042–139045.

See http://www.rsc.org/suppdata/dt/b0/b008511l/ for crystallographic data in CIF or other electronic format.

Spectrophotometric titrations

A solution containing the ligand bpia (0.1 mmol L^{-1}) in methanol (2 mL) was titrated in portions of 0.2 equivalent with a solution of $Fe(ClO_4)_3 \cdot 9H_2O$ in methanol. The same amount of iron solution was added to the solvent containing reference cuvette. After addition of the metal solution thermodynamic equilibrium was reached instantly. A complex solution (2 mL) in methanol (0.25 mmol L^{-1} for $Fe(ClO_4)_3 \cdot 9H_2O$ and the ligand bpia as well as two equivalents of piperidine) was titrated with a solution of tetrachlorocatechol monohydrate (in steps of 0.2 equivalent). After each addition the thermodynamic equilibrium was reached instantly. 2 mL of a complex solution (0.5 mmol L^{-1} for $Fe(ClO_4)_3 \cdot 9H_2O$ and the ligand bpia in methanol) were treated with one equivalent of the catechol. This solution was titrated with piperidine (0.02 mol L^{-1}; up to 4 equivalents of base) and the decomposition of the catecholate monitored by UV/Vis spectroscopy.

Table 7 The equivalents of base needed for the dioxygenation reactions of the catechols mediated by the $[Fe(L)]^{3+}$ complexes

Complex	H_2dbc	H_2moc	H_2bc	H_2mc	H_2cat
$[Fe(bpia)]^{3+}$	2.0	2.0	2.5	2.0	2.5
$[Fe(bpba)]^{3+}$	2.0	2.1	2.3	2.1	2.0
$[Fe(bipa)]^{3+}$	2.5	2.5	2.3	2.0	2.0
$[Fe(me_1tpa)]^{3+}$	2.4	2.0	2.3	2.0	2.1
$[Fe(bpqa)]^{3+}$	2.3	2.0	—[a]	—[a]	—[a]

[a] No experiments were carried out for these systems due to very small reaction rates.

Determination of the catechol 1,2-dioxygenase activity

The catechol cleaving activities of the *in situ* prepared complexes were tested according to a procedure described elsewhere.[12] To 2 mL of a 5×10^{-4} mol L^{-1} solution consisting of $Fe(ClO_4) \cdot 9H_2O$ and the ligand were added 0.02 mL of a 5×10^{-2} mol L^{-1} (1 equivalent) solution of catechol. For each complex the amount of base yielding the highest reaction rate possible was determined according to the spectrophotometric titration described above (individually for each catecholate complex using piperidine as base). The equivalents of base needed for each reaction are listed in Table 7. Then the disintegration of the complexes was followed at least three times by UV/Vis spectroscopy.

Catalytic cleavage of catechols

An excess of the catechol (0.2 mmol or 2 mmol) was added to a solution consisting of equimolar amounts of the ligand and $Fe(ClO_4)_3 \cdot 9H_2O$ (0.02 mmol in *ca.* 1 ml solvent). Immediately after this addition two equivalents of piperidine (0.04 mmol with respect to Fe) were added and the reaction mixture was stirred vigorously. Only the cleavage of the rapidly reacting catechols 3,5-di-*tert*-butylcatechol (using CD_3CN as solvent) and 3-methoxycatechol (using CD_3OD as solvent) was determined. The reactions with a tenfold excess of catechol were

monitored by ^{1}H NMR spectroscopy. Yields of the cleavage (10 and 1% catalyst) of at least three independent experiments were determined by ^{1}H NMR spectroscopy using nitromethane as standard (singlet at δ 4.3; 0.2 mmol).

Identification of the dioxygenated products

2 equivalents piperidine were added with stirring to a reaction mixture (10 mL methanol) consisting of $Fe(ClO_4)_3 \cdot 9H_2O$, the tripodal ligand, and catechol (0.2 mmol). After all catechol had reacted (monitored by TLC) the solvent was evaporated under reduced pressure at ambient temperature. The cleavage products were separated from this residue by column chromatography (SiO_2; H_2dbc, CH_2Cl_2–$CHCl_3$ 1 : 2; all other substrates, methanol). After evaporation of the solvent the products were dried *in vacuo* and identified by ^{1}H NMR or mass spectrometry. 3,5-Di-*tert*-butyl-1-oxacyclohepta-3,5-diene-2,7-dione **I**: ^{1}H NMR (300 MHz, $CDCl_3$) δ 1.15 (s, 9 H, $C(CH_3)_3$), 1.27 (s, 9 H, $C(CH_3)_3$), 6.12 (m, 1 H, CH) and 6.42 (m, 1 H, CH). 2-Methoxyhexa-2,4-dienedioic acid monomethyl ester **II**, **III**: ^{1}H NMR (300 MHz, DMSO-d_6) δ 3.68 (s, 3H, CO_2CH_3), 3.81 (s, 3H, OCH_3), 5.74 (d, 1H, CH), 7.10 (t, 1H, CH) and 7.74 (d, 1H, CH). (2-*tert*-Butyl-5-oxo-2,5-dihydrofuran-2-yl)acetic acid methyl ester **IV** (R^2 = *tert*-butyl): ^{1}H NMR (300 MHz, $CDCl_3$) δ 1.01 (s, 9 H, $C(CH_3)_3$), 2.95 (m, 2 H, CH_2CO_2), 3.64 (s, 3 H, OCH_3), 6.09 (d, 1 H, CH) and 7.51 (d, 1 H, CH). (2-Methyl-5-oxo-2,5-dihydrofuran-2-yl)acetic acid methyl ester **IV** (R^2 = methyl): ^{1}H NMR (300 MHz, $CDCl_3$) δ 2.01 (s, 3 H, CH_3), 2.91 (m, 2 H, CH_2CO_2), 3.66 (s, 3 H, OCH_3), 6.03 (d, 1 H, CH) and 7.65 (d, 1 H, CH). (3-*tert*-Butyl-5-oxo-2,5-dihydrofuran-2-yl)acetic acid methyl ester **V** (R^2 = *tert*-butyl) ^{1}H NMR (300 MHz, $CDCl_3$) δ 1.26 (s, 9 H, $C(CH_3)_3$), 2.55 (dd, 1 H, CH_2), 3.05 (dd, 1 H, CH_2), 3.71 (s, 3 H, OCH_3), 5.40 (m, 1 H, OCH) and 5.85 (d, 1 H, CH). (3-Methyl-5-oxo-2,5-dihydrofuran-2-yl)acetic acid methyl ester **V** (R^2 = methyl): ^{1}H NMR (300 MHz, $CDCl_3$) δ 2.26 (s, 3 H, CH_3), 2.61 (dd, 1 H, CH_2), 2.85 (dd, 1 H, CH_2), 3.71 (s, 3 H, OCH_3), 5.22 (m, 1 H, OCH) and 5.84 (m, 1 H, CH). (5-Oxo-2,5-dihydrofuran-2-yl)acetic acid methyl ester **VI**: MS *m*/*z*, 157 $[MH]^+$.

Acknowledgements

Financial support from the Henkel KGaA, Degussa-Hüls AG, the Deutsche Forschungsgemeinschaft, the Katalyseverbund NRW, and the Fonds der Chemischen Industrie is gratefully acknowledged. M. P. thanks the Ministerium für Schule und Weiterbildung, Wissenschaft und Forschung des Landes Nordrhein-Westfalen for a Graduiertenstipendium.

References

1 L. Que, Jr. and R. Y. N. Ho, *Chem. Rev.*, 1996, **96**, 2607.
2 J. D. Lipscomb and A. M. Orville, *Metal Ions Biol. Syst.*, 1992, **28**, 243; T. Senda, K. Sygiyama, H. Narita, T. Yamamoto, K. Kimbara, M. Fukuda, M. Sato, K. Yano and Y. Mitsui, *J. Mol. Biol.*, 1996, **255**, 735; D. H. Ohlendorf, J. D. Lipscomb and P. C. Weber, *Nature* (*London*), 1988, **336**, 403; L. Que, Jr., *Iron Carriers and Iron Proteins*, ed. T. M. Loehr, VCH, New York, 1989.
3 S. J. Lange and L. Que, Jr., *Curr. Opin. Chem. Biol.*, 1998, **2**, 159.
4 L. Que, Jr., *Bioinorganic Catalysis*, eds. J. Reedijk and E. Bouwman, 2nd edn., Marcel Dekker Inc., New York, Basel, 1999.
5 T. Funabiki, *Oxygenases and Model Systems*, ed. T. Funabiki, Kluwer Academic Publishers, Dordrecht, Boston, London, 1997.
6 L. Que, Jr., R. C. Kolanczyk and L. S. White, *J. Am. Chem. Soc.*, 1987, **109**, 5373; D. D. Cox and L. Que, Jr., *J. Am. Chem. Soc.*, 1988, **110**, 8085.
7 L. Que, Jr., J. D. Lipscomb, E. Münck and J. M. Wood, *Biochim. Biophys. Acta*, 1977, **485**, 60.
8 T. Funabiki and T. Yamazaki, *J. Mol. Catal. A*, 1999, **150**, 37.
9 H. G. Jang, D. D. Cox and L. Que, Jr., *J. Am. Chem. Soc.*, 1991, **113**, 9200.
10 W. O. Koch and H.-J. Krüger, *Angew. Chem.*, 1995, **107**, 2929; W. O. Koch and H.-J. Krüger, *Angew. Chem., Int. Ed. Engl.*, 1995, **34**, 2671.
11 Y.-M. Chiou and L. Que, Jr., *Inorg. Chem.*, 1995, **34**, 3577; T. Ogihara, S. Hikichi, M. Akita and Y. Moro-oka, *Inorg. Chem.*, 1998, **37**, 2614; T. Funabiki, T. Yamazaki, A. Fukui, T. Tanaka and S. Yoshida, *Angew. Chem.*, 1999, **110**, 527; T. Funabiki, T. Yamazaki, A. Fukui, T. Tanaka and S. Yoshida, *Angew. Chem., Int. Ed. Engl.*, 1999, **37**, 513; R. Viswanathan and M. Palaniandavar, *J. Chem. Soc., Dalton Trans.*, 1995, 1259; H. Weiner and R. G. Finke, *J. Am. Chem. Soc.*, 1999, **121**, 9931; P. Mialane, J.-J. Girerd, J. Guilhem and L. Tchertanov, *Inorg. Chim. Acta*, 2000, **299**, 39.
12 P. Mialane, L. Tchertanov, F. Banse, J. Sainton and J.-J. Girerd, *Inorg. Chem.*, 2000, **39**, 2440.
13 M. Pascaly, M. Duda, A. Rompel, B. H. Sift, W. Meyer-Klaucke and B. Krebs, *Inorg. Chim. Acta*, 1999, **291**, 289.
14 M. Pascaly, Ç. Nazikkol, F. Schweppe, A. Wiedemann, K. Zurlinden and B. Krebs, *Z. Anorg. Allg. Chem.*, 2000, **626**, 50.
15 Y. Nishida, H. Shimo and S. Kida, *J. Chem. Soc., Chem. Commun.*, 1994, 1611.
16 R. Viswanathan, M. Palaniandavar, T. Balasubramanian and T. P. Mutiah, *Inorg. Chem.*, 1999, **37**, 2943.
17 T. Funabiki, A. Mizoguchi, T. Sugimoto, S. Tada, M. Tsuji, H. Sakamoto and S. Yoshida, *J. Am. Chem. Soc.*, 1996, **109**, 2921; T. Funabiki, M. Ishikawa, Y. Nagai, J. Yorita and S. Yoshida, *J. Chem. Soc., Chem. Commun.*, 1994, 1951; T. Funabiki, I. Yoneda, M. Ishikawa, M. Ujiie, Y. Nagai and S. Yoshida, *J. Chem. Soc., Chem. Commun.*, 1994, 1453.
18 M. G. Weller and U. Weser, *J. Am. Chem. Soc.*, 1992, **104**, 3752; M. G. Weller and U. Weser, *Inorg. Chim. Acta*, 1995, **107**, 243.
19 M. Duda, M. Pascaly and B. Krebs, *Chem. Commun.*, 1997, 935.
20 F. Schweppe, H. Sirges, M. Pascaly, M. Duda, Ç. Nazikkol, W. Steinforth and B. Krebs, *Peroxide Chemistry. Mechanistic and Preparative Aspects of Oxygen Transfer*, ed. W. Adam, Wiley-VCH, Weinheim, 2000, p. 232.
21 M. Pascaly, F. Schweppe and B. Krebs, *J. Inorg. Biochem.*, 1999, **74**, 260.
22 H. Nagao, N. Komeda, M. Mukaida, M. Suzuki and K. Tanaka, *Inorg. Chem.*, 1996, **35**, 6909.
23 N. Wei, N. N. Murthy, Q. Chen, J. Zubieta and K. D. Karlin, *Inorg. Chem.*, 1994, **33**, 1953.
24 N. Wei, N. N. Murthy, Z. Tyeklár and K. D. Karlin, *Inorg. Chem.*, 1994, **33**, 1177.
25 W. O. Koch, V. Schünemann, M. Gerdan, A. X. Trautwein and H.-J. Krüger, *Chem. Eur. J.*, 1998, **4**, 1255.
26 R. L. Carlin, *Magnetochemistry*, Springer Verlag, Berlin, Heidelberg, New York, Tokyo, 1986; O. Kahn, *Molecular Magnetism*, VCH Verlag, Weinheim, New York, Cambridge, 1993.
27 M. M. Maltempo, *J. Chem. Phys.*, 1974, **61**, 2540; E. L. Bominaar and R. Block, *J. Chem. Phys.*, 1991, **95**, 6712; C. A. Reed and F. Guiset, *J. Am. Chem. Soc.*, 1996, **118**, 3281; S. Mitra, V. R. Marathe and R. Birdy, *Chem. Phys. Lett.*, 1983, **96**, 103.
28 M. D. Stallings, M. M. Morrison and D. T. Sawyer, *Inorg. Chem.*, 1981, **20**, 2655.
29 M. E. Nabi, M. A. Islam and A. H. Khan, *J. Bangl. Acad. Sci.*, 1998, **22**, 285; M. Born, P.-A. Carrupt, R. Zinn, F. Brée, J.-P. Tillement, K. Hostettmann and B. Testa, *Helv. Chim. Acta*, 1996, **79**, 1147; D. Nematollahi and S. M. Golabi, *J. Electroanal. Chem.*, 1996, **405**, 133.
30 *Gmelins Handbuch der Anorganischen Chemie*, Sauerstoff, 8. Auflage, Verlag Chemie, Weinheim, 1958.
31 We were able to obtain single crystals of a dinuclear iron(III) complex from one solution utilized in the NMR dioxygenation experiments. The structural features of the complex $[Fe_2(\mu\text{-O})(bpba)_2Cl_2][ClO_4]_2$ are very similar to those of $[Fe_2(\mu\text{-O})(bpia)_2Cl_2]Cl_2 \cdot 4MeOH$ with antiferromagnetically coupled iron(III) centers described in ref. 13. The complete details of this compound are under current investigation.
32 B. Rieger, A. S. Abu-Surrah, R. Fawzi and M. Steiman, *J. Organomet. Chem.*, 1995, **497**, 73.
33 M. A. Phillips, *J. Chem. Soc.*, 1929, **172**, 2393; E. S. Lane, *J. Chem. Soc.*, 1957, 3313; L. A. Cescon and A. R. Day, *J. Org. Chem.*, 1962, **27**, 591.
34 G. M. Sheldrick, SHELXS 97, Program for Crystal Structure Determination, University of Göttingen, 1997.
35 G. M. Sheldrick, SHELXL 97, Program for Crystal Structure Refinement, University of Göttingen, 1997.